JGR Oceans

RESEARCH ARTICLE
10.1029/2020JC016840

Special Section:
Years of the Maritime Continent

Biweekly Mixed Rossby-Gravity Waves in the Equatorial Indian Ocean

Kandaga Pujiana[1,2,3] and Michael J. McPhaden[1]

[1]NOAA Pacific Marine Environmental Laboratory, Seattle, WA, USA, [2]Faculty of Earth Sciences and Technology, Bandung Institute of Technology, Bandung, Indonesia, [3]Now at Cooperative Institute for Marine and Atmospheric Studies of University of Miami and NOAA Atlantic Oceanographic and Meteorological Laboratory, Miami, FL, USA

Key Points:

- Biweekly variations are prominent in moored buoy velocity and satellite sea level measurements in the equatorial Indian Ocean
- The properties of these biweekly oscillations are consistent with wind-forced mixed Rossby-gravity waves
- Phase propagation of the biweekly Rossby-gravity waves is westward and upward while energy propagation is eastward and downward

Correspondence to:
K. Pujiana,
kandaga.pujiana@noaa.gov

Citation:
Pujiana, K., & McPhaden, M. J. (2021). Biweekly mixed Rossby-gravity waves in the equatorial Indian Ocean. *Journal of Geophysical Research: Oceans*, *126*, e2020JC016840. https://doi.org/10.1029/2020JC016840

Received 29 SEP 2020
Accepted 13 MAR 2021

Abstract This study describes biweekly (defined as periods between 10 and 15 days) ocean variability in relation to equatorial wave theory using a comprehensive set of moored ocean current velocities as well as satellite-retrieved oceanic and atmospheric parameters in the Indian Ocean. Moored biweekly current velocities exhibit the meridional structure of mixed Rossby-gravity waves: Symmetric for meridional velocity and antisymmetric for zonal velocity around the equator with a decay scale of 228–309 km. The biweekly meridional velocity along the equator has average zonal and vertical wavelengths of 3,430 ± 550 km and 0.76 ± 0.15 km, respectively, with phase propagating westward at speeds of 2.8–3.1 m s^{-1} and upward at 54–56 m day^{-1}. Conversely, wave energy is inferred to propagate eastward and downward. The range of best fit constants (1.4–2.0 m s^{-1}) that result from the linear separation of horizontal and vertical wave structures suggests the second baroclinic wave mode is dominant over other low baroclinic modes in accounting for the velocity variability. The biweekly waves are forced by surface winds; satellite-derived wind stress, sea level, and surface current anomalies, regressed against the first principal component of the biweekly moored velocities, illustrate the basin-scale structure and temporal evolution of the waves.

Plain Language Summary An extensive set of moored ocean current velocities permits evaluation of the three-dimensional flow field properties, dynamics, and energetics of biweekly waves in the Indian Ocean. We determine, for the first time, the meridional structure of the biweekly flow field from the multiyear in situ measurements and demonstrate that it is dynamically consistent with that of Rossby-gravity waves, with zonal velocity being antisymmetric and meridional velocity being symmetric about the equator. Our analysis finds that the waves have a decay scale of 228–309 km away from the equator in the meridional direction, a zonal wavelength of 3,430 ± 550 km, and vertical wavelength of 0.76 ± 0.15 km. Phase propagates westward at speeds of 2.8–3.1 m s^{-1} and upward at 54–56 m day^{-1}, while wave energy flux is eastward and downward. A combination of moored velocities and satellite-derived data illustrates the basin-scale structure and temporal evolution of the waves in the Indian Ocean.

1. Introduction

The tropical Indian Ocean exhibits a host of wind-forced oceanic phenomena across a broad spectrum of timescales from days to years that are fundamental in regulating ocean-atmosphere interactions and climate on both regional and global scales. Most notable are the seasonally reversing ocean currents driven by Asian monsoon winds (e.g., Schott et al., 2009) and the unique surface eastward jet that appears twice a year along the equator in response to energetic westerlies during the transitions between the Northeast and Southwest monsoons (e.g., McPhaden, 1982; Wyrtki, 1973). Another unique feature of the circulation is the seasonal cross-equatorial meridional overturning circulation, with frictional flow at the surface toward the winter hemisphere in the open ocean and a return flow in the thermocline below (Miyama, McCreary, Jensen, et al., 2003; Wang & McPhaden, 2017). Embedded within this monsoon wind-driven circulation are intraseasonal variations associated with the atmospheric Madden-Julian oscillation (MJO) (e.g., Zhang, 2013) that excite large-scale oceanic responses in terms of equatorial waves and mixed layer dynamics (e.g., Nagura & McPhaden, 2008; Pujiana et al., 2018).

Although not as well studied as the above phenomena, near surface variations in the biweekly period band are very prominent. Reppin et al. (1999), using near-surface current meter data at 80.5°E and on the equator

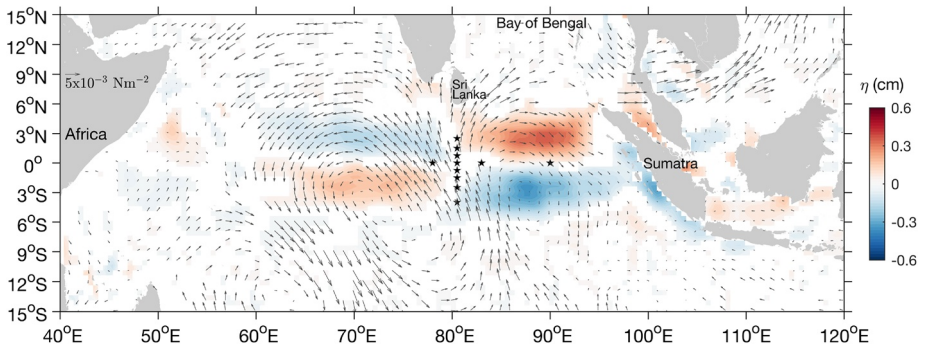

Figure 1. Regressed sea level anomaly (η; shading) and wind stress (τ; arrows) at biweekly (10–15 days) periods against the principal component of the first bivariate empirical orthogonal function (EOF) of u and v averaged in the upper 150 m at the 80.5°E moorings in the Indian Ocean. The regressed values are at zero lag and scaled to one standard deviation of the principal component. Omitted wind stress values are below a 95% significance level. Stars mark the RAMA moorings.

extending between July 1993 - September 1994, first reported a maximum variance at 15.5 days in the meridional velocity (v) but not in the zonal velocity (u). More recent moored observations at 83°E and 90°E confirmed the significance of biweekly variations in v on the equator (Masumoto et al., 2005; Sengupta et al., 2004). Satellite-derived sea level and surface salinity anomalies also demonstrate significant biweekly variations in the Indian Ocean (Arzeno et al., 2020; Roman-Stork et al., 2020; Subrahmanyam et al., 2018). Biweekly variations are evident in other equatorial basins as well where they have been documented in a variety of analyses (Farrar & Durland, 2012; Shinoda, 2010; Weisberg et al., 1979; Zhu et al., 1998).

Model-based dynamical studies indicate that much of the observed biweekly variability in the Indian Ocean, as in the other tropical ocean basins, can be interpreted in terms of mixed Rossby-gravity waves (Miyama et al., 2006; Nagura et al., 2014; Ogata et al., 2008; Sengupta et al., 2004). The Rossby-gravity waves are forced by the winds attributed to the atmospheric quasi-biweekly mode (QBM) (Kikuchi & Wang, 2009). The QBM has the meridional structure of an atmospheric equatorial Rossby wave, with a zonal wavelength on the order of 6,000 km and a westward phase speed of 4–5 m s^{-1}. The low-level wind manifestation of the QBM in the tropical Indian Ocean exhibits a double vortex structure, with a vortex centered near 3°S and the other one centered at about 15°N-20°N (Chen & Chen, 1993). Together with the MJO, the QBM influences the active and break conditions of the Indian boreal summer monsoon and the Australian–Indonesian boreal winter monsoon (Krishnamurti & Ardanuy, 1980; Wheeler & McBride, 2005).

We here build upon previous investigations of biweekly variations in the Indian Ocean by evaluating their kinematics, dynamics, and energetics using ocean velocity data from an array of acoustic Doppler current profiler (ADCP) moorings (Figure 1). This is the most comprehensive moored velocity data set available to date in the Indian Ocean, spanning 2.5°N-4°S along 80.5°E and the equator from 78°E to 90°E. From the meridional array, we derive the meridional structure of the biweekly flow field for the first time from in situ measurements and test whether it is dynamically consistent with that of mixed Rossby-gravity waves expected from theory. The multiyear velocity profiles at several moorings zonally separated along the equator allow assessment of the vertical structure, zonal and vertical propagation of phase and energy, and kinetic energy flux of the biweekly waves. Aided by satellite and reanalysis products, we also examine the biweekly mixed Rossby-gravity wave's basin-scale structure and how it corresponds with the flow fields inferred from the moored velocities. Our interpretation of the moored velocity and satellite-derived data in terms of Rossby-gravity wave theory extends the results of past studies that are exclusively based on either satellite products (e.g., Arzeno et al., 2020), sparser mooring data (e.g., Sengupta et al., 2004), or numerical experiments (Miyama et al., 2006).

We proceed in Section 2 by describing the data. In Sections 3 and 4, we discuss the kinematics of the biweekly flow field inferred from moored observations and assess comparisons between the observed flow field and the dynamics of mixed Rossby-gravity waves expected from theory, including meridional and vertical structures, dispersion characteristics, and energetics. In Section 5, we examine the basin-scale structure of the

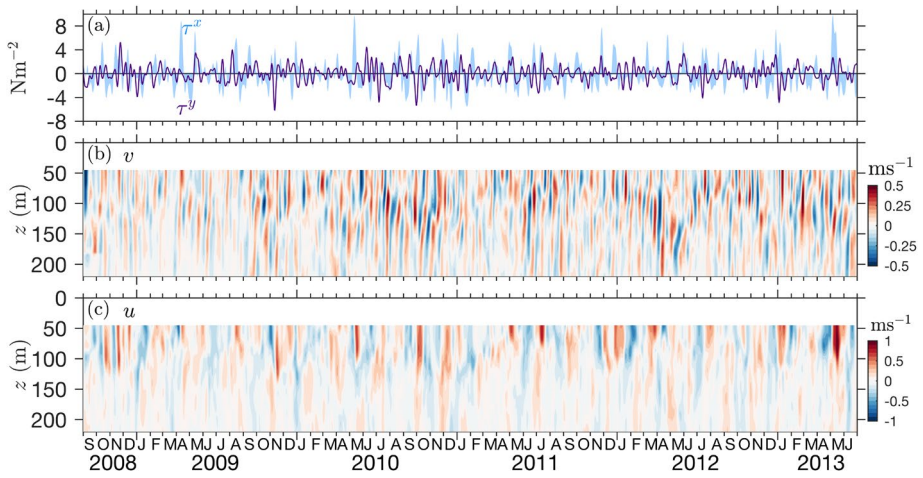

Figure 2. Daily averages of (a) satellite-retrieved zonal wind stress [τ^x] and meridional wind stress [τ^y], (b) moored v, and (c) u on the equator at 80.5°E between September 2008 and June 2013. The daily averages were band-passed filtered with cut-off frequencies of 0.0099–0.111 cycle day^{-1} to isolate the intraseasonal variability between 10 and 100 days. The intraseasonal τ^x and τ^y are area-averaged data over an area within latitudes of 1°N-1°S and longitudes of 79°E-81°E.

biweekly mixed Rossby-gravity waves in the Indian Ocean using satellite-derived and reanalysis products. We then conclude with a summary and discussion.

2. Data and Methods

The three-dimensional properties of the biweekly flow field and their interpretation in terms of mixed Rossby-gravity wave in the equatorial Indian Ocean are evaluated with hourly u and v obtained from an array of subsurface moorings equipped with upward-looking ADCPs along 80.5°E and on the equator between 78°E and 90°E (Figure 1). The observations are embedded within the Research Moored Array for African-Asian-Australian Monsoon Analysis and Prediction (RAMA; McPhaden et al., 2009; McPhaden et al., 2015). Sampling characteristics of the ADCP have been described in detail in McPhaden et al. (2015) and Pujiana and McPhaden (2020).

We focus on the observed horizontal velocities in the upper 220 m during the nearly 5-year period of September 2008–June 2013 during which the moorings were synchronously operational. Velocities between the surface down to 40 m are neglected because of contamination of the velocity measurements from backscatter off the surface. Similarly, the horizontal velocities deeper than 220 m are also not used in the present study as they were not consistently observed at all moorings. The data between 40 and 220 m are available at 5 m vertical resolution. For more details about the velocity measurements at the moorings, readers can refer to Pujiana and McPhaden (2020).

Major gaps in the horizontal currents at the moorings along 80.5°E were filled using data from nearby moorings via linear regression (Johnson & McPhaden, 1993), a gap-filling method that McPhaden et al. (2015) validated for the Indian Ocean array by comparing filled time series with observed time series for periods when no gaps existed. Minor gaps with a length up to a few days between deployments were filled by linear interpolation. Results from analyses of daily averages of the hourly horizontal velocities are reported in this study, and a subset of the daily averages is shown in Figure 2.

In addition to the measurements from the RAMA moorings, we examined satellite-derived surface currents, wind stress (τ), and η over the Indian Ocean to gain insights into the basin-scale structure of the biweekly variations identifiable from the moorings. We employed the daily, 0.25° latitude × 0.25° longitude gridded τ, η, and surface current data respectively from the near real-time Institut Français de Recherche pour l'exploitation de la Mer (IFREMER; Bentamy et al., 2002), Archiving and Validation and Interpretation of Satellite Oceanographic (AVISO), and Geostrophic and Ekman Current Observatory (GEKCO; Sudre et al., 2013) products.

The GEKCO velocity product combines geostrophic and Ekman flows using AVISO global η data to determine the geostrophic component and the mean wind field data from QuikSCAT satellite to compute the Ekman component. The GEKCO velocities have been validated against the in situ velocities from moored and shipboard ADCPs and drifters over the global ocean and are generally in agreement with the observed velocities (Sudre et al., 2013).

Compared to the daily averages of the moored velocities at 40 m at the RAMA moorings, the GEKCO currents show a statistically significant correlation (p-value < 0.05) with the velocities at most of the mooring sites, with the correlation coefficient (r) between 0.56 and 0.73 for u and between 0.11 and 0.33 for v. Evident across all tropical basins particularly on the equator, u shows a larger degree of correlation than v (Sudre & Morrow, 2008; Sudre et al., 2013). Sudre and Morrow (2008) argued that the cause of the lower correlations for v is likely due to an aliasing problem in the geostrophic component of the currents, which are determined from altimetry data sampled with a Nyquist frequency of 1/20 days.

We performed a normal mode decomposition of an average Brunt-Väisälä frequency (N) vertical profile based on Argo profiles and other shipboard hydrographic data in the region 5°N-5°S and 76°E-92°E to determine vertical mode structures and separation constants, equivalent to long gravity wave phase speeds. The separations constants were 2.6, 1.6, 1.0, and 0.7 m s^{-1}, respectively, for the first four baroclinic modes. These values are comparable to those determined by Nagura and McPhaden (2010) in the same region from similar data, namely 2.5, 1.55, 0.99, and 0.74 m s^{-1}.

We applied a number of time series and spatial analysis methods to the moored and satellite-retrieved data to extract the biweekly signals. To estimate the relative fraction of variance of the biweekly band compared to other band of frequencies, we used a multi-taper method with adaptive weighing to determine the spectral estimates of the data (Percival & Walden, 1993). Isolating the variability of the biweekly band and other frequency bands from the data was achieved using a fourth order band-pass Butterworth filter.

Our definition of "biweekly" encompasses variations at periods of 10–15 days for reasons that will become apparent in the next section. This is a slightly narrower period band than the 10–20 day band used by Sengupta et al. (2004), Arzeno et al. (2020), and others. However, we will show that none of our results fundamentally change if we use 10–20 days as a definition of "biweekly," so our results can be compared to previous studies without loss of generality.

We analyzed the band-pass filtered biweekly data to assess the spatial structures of the biweekly mode using empirical orthogonal function (EOF) and regression methods (Thomson & Emery, 2014). To estimate the zonal and vertical wavenumbers of the biweekly wave, we applied a coherence analysis (Thomson & Emery, 2014) to the moored velocities at multiple pairs of moorings separated zonally and vertically on the equator. Based on the phase lags determined from the coherence analysis, we derived wavenumbers which then were used to estimate the dispersion relation of the biweekly mode.

3. Biweekly Horizontal Velocity Spatial Structure

We first band-pass the data at intraseasonal (10–100 day) periods to illustrate the differences between zonal and meridional winds and ocean velocities at these frequencies. The band-passed data show that biweekly variability is prominent in meridional wind stress (τ^y) and v on the equator, while monthly and longer variations control the variability of the zonal component (Figure 2). An energetic eastward equatorial jet with a speed up to 1 m s^{-1} occurs at a period of 1–2 months in the upper 150 m (Figure 2c) in response to eastward zonal wind stress (τ^x) varying with a similar timescale (Figure 2a). The eastward acceleration of the near-surface layer at the equator is related to MJO atmospheric forcing consistent with previous analyses of intraseasonal variability in zonal velocities (e.g., Nagura & McPhaden, 2010).

Meridional velocity shows a pronounced biweekly variability along the equator in the central and eastern Indian Ocean. The variance preserving spectra of v observed at the equatorial moorings show that biweekly variability is predominant in the intraseasonal period band and strongest in the upper 150 m (Figures 3a–3d). For the moorings between 78°E and 83°E, biweekly variability in the period band 10–15 days accounts for 52%–59% of the total intraseasonal variance of v averaged in the upper 150 m. At the easternmost mooring at 90°E, biweekly variance is confined closer to the surface and weaker (Figure 3d), accounting for 47%

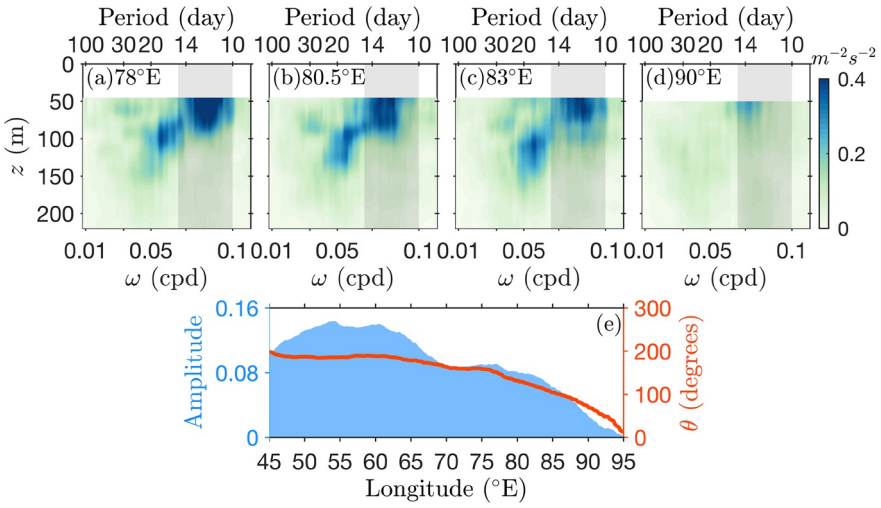

Figure 3. (a–d) Variance preserving spectra of v observed at the equatorial moorings from September 2008 to June 2013. (e) Amplitude (blue) and phase (θ; red) of the leading complex EOF mode of biweekly τ^y variability averaged between 1°N and 1°S. The leading complex EOF mode accounts for 31% of the biweekly τ^y variance. Gray shades mark the periods between 10 and 15 days.

of the total intraseasonal variance. For comparison, the biweekly variability explains only 7%–12% of the total intraseasonal variance in depth-averaged u along the equator.

The zonal variation along the equator of the biweekly energy in v, increasing from the eastern to the central basin, is consistent with that of the biweekly τ^y. The amplitude of the first complex EOF mode of the observed biweekly τ^y, averaged within 1°N-1°S, gradually increases from the west coast of Sumatra to the central Indian Ocean along the equator peaking around 55°E-60°E before decreasing further to the west (Figure 3e). The leading complex EOF mode of biweekly τ^y accounts for 31% of the variance and shows a phase structure continuously increasing to the west along the equator, suggesting westward propagation of the biweekly wind (red curve in Figure 3e). This relationship between τ^y and v along the equator is consistent with previous studies that reported a strong relationship between the two parameters at biweekly periods in the equatorial Indian Ocean (Miyama et al., 2006; Ogata et al., 2008; Sengupta et al., 2004).

We note that there is a shift in observed variance in meridional velocity with depth, with the largest variance at periods between 10 and 15 days in the upper 100 m but centered near 20 days at depths of 100–150 m. It is unclear whether variations in these two period bands are related, given their distinct vertical distributions. We would expect locally wind-forced variability to be largest at the surface, which is the case for variations at periods between 10 and 15 days but not for those at periods centered around 20 days. The signal near 20 days may be related to the shorter period fluctuations or it could be the manifestation of the instability of the large-scale circulation. In view of this uncertainty, we concentrate on the narrower 10–15 day band in the analysis that follows.

The meridional structure of biweekly energy is illustrated in the depth-averaged velocity spectra along 80.5°E (Figure 4). We see that that the biweekly variance in $\overline{v}$ decays off the equator, in contrast to that of $\overline{u}$ which is least energetic on the equator (Figures 4a–4h). The spectra of $\overline{u}$ and $\overline{v}$ within the biweekly period band are not significantly different at 2.5°N, 2.5°S, and 4°S (Figures 4a, 4g, and 4h). The spectral ratio of $\overline{v}$ to $\overline{u}$, $E_{\left(\frac{\overline{v}}{\overline{u}}\right)} = \frac{\overline{S_{\overline{v}}}}{\overline{S_{\overline{u}}}}$, averaged over a period band of 10–15 days, clearly indicates that meridional kinetic energy significantly exceeds the zonal component on the equator, while they are comparable at the northern and southernmost mooring sites (Figure 4i).

The relative spectral amplitudes of $\overline{u}$ and $\overline{v}$ averaged in the biweekly period band indicate the meridional structure of the biweekly mode (Figure 4). To further explore this meridional structure and compare it

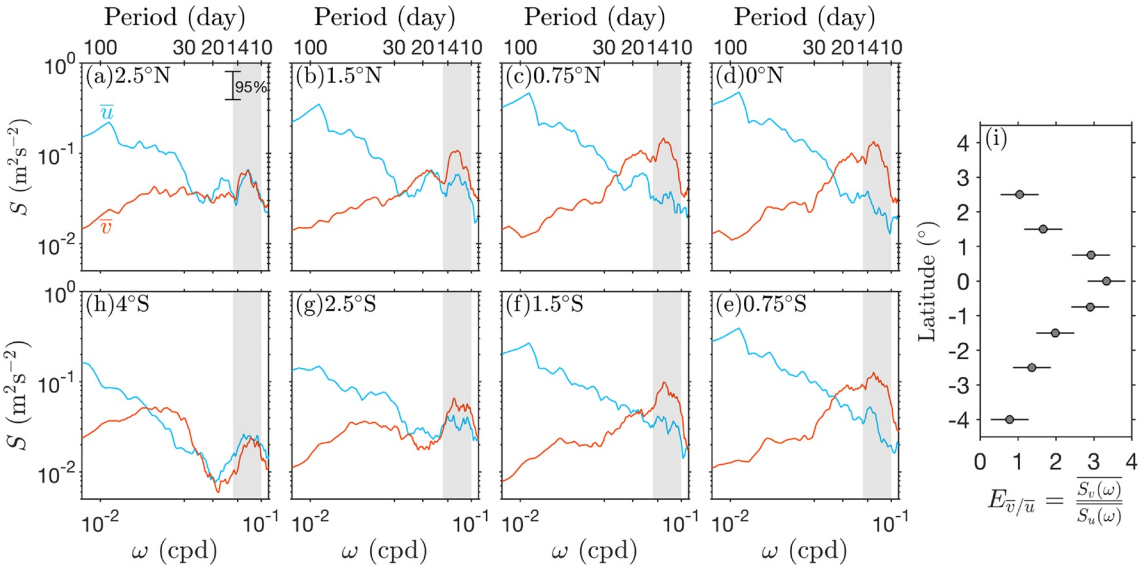

Figure 4. (a–h) Variance preserving spectra of $\overline{u}$ (blue) and $\overline{v}$ (red), where the overbar denotes depth average in the upper 150 m, at the moorings along 80.5°E. Gray shades mark the period band of 10–15 days. (i) The ratio of the spectra of $\overline{v}$ over the spectra of $\overline{u}$ averaged within the 10–15 day period band. Horizontal lines denote the uncertainty of the ratio based on the chi-square 95% confidence limits of the spectra.

to theoretical expectations, we applied a multivariate EOF to the 10–15 day band-pass filtered $\overline{u}$ and $\overline{v}$ data. The leading bivariate EOF mode (Figure 5), accounting for about 40% of the band-passed variance, shows that the meridional structures of the biweekly mode in horizontal velocities are indeed consistent with that of mixed Rossby-gravity wave, with $\overline{u}$ being antisymmetric and $\overline{v}$ being symmetric around the equator.

To compare the observed meridional structure with the theoretical structure expected for mixed Rossby-gravity wave in more detail, we fit $\overline{v}$ and $\overline{u}$ meridional structures to the real part of the eigenfunctions of the orthogonal horizontal velocity components for mixed Rossby-gravity wave, expressed as

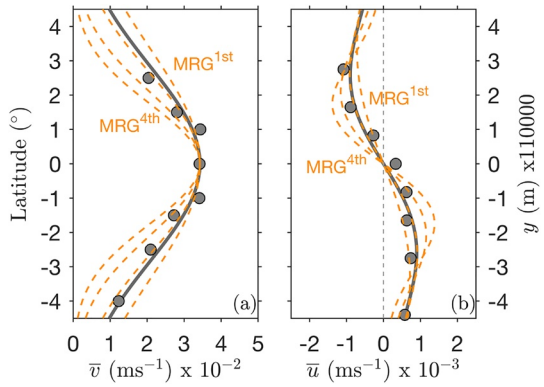

Figure 5. Dots indicate the first bivariate EOF mode for the observed (a) $\overline{v}$ and (b) $\overline{u}$ band-pass filtered at 10–15 days at the moorings along 80.5°E. Solid curves indicate the least squares fit to the observed values, using the meridional function of the respective horizontal current component for theoretical mixed Rossby-gravity wave. The inferred values of c from the fits are 1.8 ± 0.4 m s^{-1} and 1.6 ± 0.4 m s^{-1} for $\overline{v}$ and $\overline{u}$, respectively, with the uncertainty denoting the margin of error based on a 95% confidence level. Orange dashed lines denote theoretical meridional structures of the respective current component associated with the first four baroclinic Rossby-gravity wave modes.

$$\overline{v} = v_o e^{\frac{-\beta y^2}{2c}} e^{i(kx-\omega t)} \quad (1)$$

and

$$\overline{u} = \frac{i\omega y}{c} v_o e^{\frac{-\beta y^2}{2c}} e^{i(kx-\omega t)}, \quad (2)$$

where v_o is meridional velocity on the equator, $\beta = 2.3 \times 10^{-11}$ m^{-1} s^{-1} is the meridional gradient of the Coriolis parameter, y is latitude, c is the Kelvin wave phase speed (or equivalently, the constant that emerges from the separation of horizontal and vertical wave structures in the linear equations of motion), k is zonal wavenumber, x is longitude, ω is frequency, and t represents time (Gill, 1982). Allowing c and v_o to vary, the least-squares fit to $\overline{v}$ yields $v_o \sim 0.034 \pm 0.002$ m s^{-1} and $c \sim 1.8 \pm 0.4$ m s^{-1} and the least squares fit to $\overline{u}$ yields $v_o \sim 0.02 \pm 0.003$ m s^{-1} and $c \sim 1.6 \pm 0.4$ m s^{-1}, with the uncertainty denoting the margin of error based on a 95% confidence level (Figure 5, Table 1). Compared to the Rossby-gravity wave eigenfunctions of Equations 1 and 2 with the representative separation constants for the first four vertical modes (dashed curves in Figure 5), the least-squares fits closely approximate the eigenfunctions for the lowest

Table 1
Mixed Rossby-Gravity Wave Parameter Values Estimated for the 10–15 Day and 10–20 day Band-Pass Filtered Data, With Error Limits Based on 95% Confidence Levels

Period band	10–15 days	10–20 days
Values inferred from the leading EOF meridional structure mode for $\overline{u}$ and $\overline{v}$		
Separation constant (c) from $\overline{v}$	1.8 ± 0.4 ms^{-1}	1.7 ± 0.4 ms^{-1}
Separation constant (c) from $\overline{u}$	1.6 ± 0.4 ms^{-1}	1.6 ± 0.4 ms^{-1}
Values inferred from the vertical structure of v on the equator		
Vertical phase speed (c_z)	56 ± 5 $mday^{-1}$	51 ± 4 $mday^{-1}$
Values inferred from the dispersion diagram		
Separation constant (c)	2.0 ± 0.2 ms^{-1}	1.8 ± 0.2 ms^{-1}
Zonal phase speed (c_x)	2.8 ± 0.4 ms^{-1}	3.2 ± 0.4 ms^{-1}
Vertical phase speed (c_z)	54 ± 6 $mday^{-1}$	47 ± 6 $mday^{-1}$
Zonal wavelength (λ_x)	3,430 ± 550 km	3,930 ± 550 km
Vertical wavelength (λ_z)	760 ± 150 m	665 ± 150 m

two baroclinic Rossby-gravity modes inferred from our normal mode decomposition of the average N profile in the equatorial band.

Rotary spectral analysis of the velocity vector, $\overline{u}\hat{x} + \overline{v}\hat{y}$ (where $\hat{x}$ and $\hat{y}$ are unit vectors in the eastward and meridional directions), that separates the velocity vector into oppositely rotating clockwise ($-\omega$) and counterclockwise ($+\omega$) components (Figures 6a–6h), shows that the spectral amplitudes of both the clockwise [$S(-\omega)$] and counterclockwise [$S(+\omega)$] components for the biweekly period band have the same magnitude on the equator (Figure 6d) but are significantly different off the equator (Figures 6a–6c and 6e–6h). To quantify the dominance of $S(-\omega)$ over $S(+\omega)$ in determining the biweekly velocity field, we computed the rotary coefficient, $r(\omega) = \dfrac{S(+\omega) - S(-\omega)}{S(+\omega) + S(-\omega)}$ (Thomson & Emery, 2014), averaged over the 10–15 day period

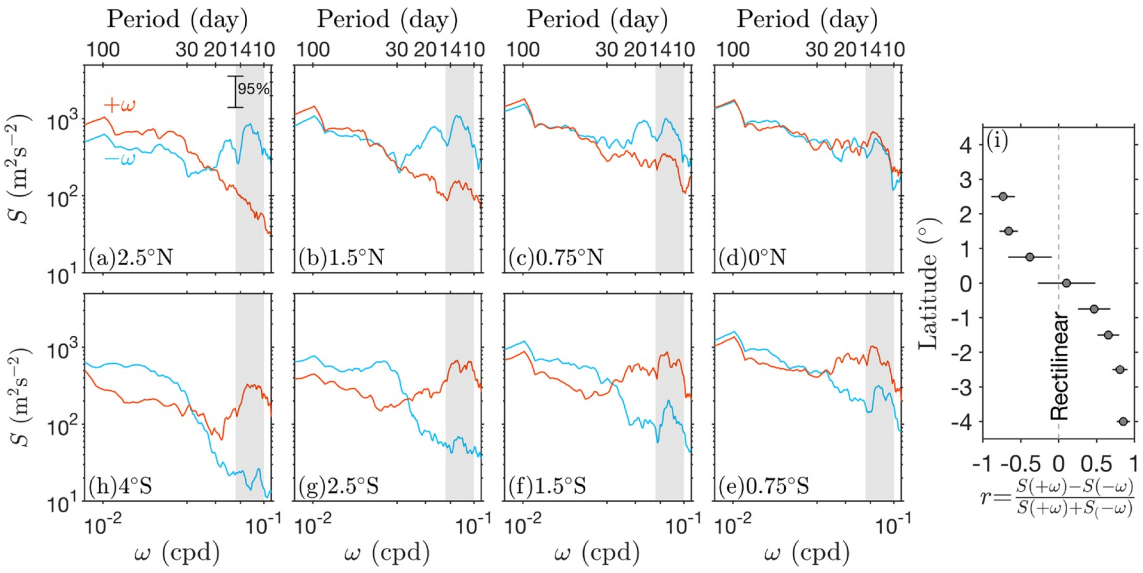

Figure 6. (a–h) Variance preserving rotary spectra of $\overline{u}\hat{x} + \overline{v}\hat{y}$ along 80.5°E, with blue and red curves respectively indicating the counterclockwise and clockwise components of the rotary spectra. Gray shading marks the 10–15 day period band. (i) Rotary coefficient averaged for the 10–15 day period band. Horizontal lines denote the uncertainty of the ratio based on the chi-square 95% confidence limits of the spectra.

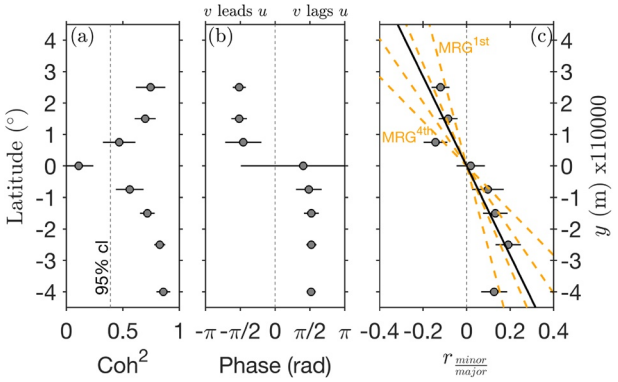

Figure 7. Mean values of (a) squared coherence amplitude and (b) phase difference between $\overline{u}$ and $\overline{v}$ at the moorings along 80.5°E for the 10–15 day period band. (c) The ratio of semi-minor over semi-major axes for horizontal currents varying at a period of 14-days, inferred from a harmonic analysis of $\overline{u}\hat{x} + \overline{v}\hat{y}$. The black line indicates the least squares fit to the ratio with a function appropriate for mixed Rossby-gravity wave as described in the text. The inferred Kelvin wave phase speed (c) from the fit to Equation 3 is 1.4 ± 0.2 m s^{-1}, with the uncertainty indicating the margin of error based on a 95% confidence level. Horizontal lines denote the 95% confidence limits based on a Monte Carlo method.

band. The rotary coefficient indicates that $S(-\omega)$ dominates the depth-averaged horizontal velocities at the moorings in the Northern Hemisphere, while $S(+\omega)$ dominates in the Southern Hemisphere (Figure 6i). It also shows both rotary components have about equal spectral amplitudes in the biweekly period band on the equator. This implies that the biweekly current motions are rectilinear or unidirectional on the equator and circularly polarized or elliptical off the equator. Moreover, the sign of the rotary coefficient is variable with latitude, negative in the Northern Hemisphere, and positive in the Southern Hemisphere. The latitudinal dependence of the orientation of the rotary coefficient of the biweekly velocities agrees with the flow field expected for mixed Rossby-gravity wave. A snapshot of the biweekly velocity field attributed to a Rossby-gravity wave is shown in Figure 10a.

A coherence analysis between $\overline{u}$ and $\overline{v}$ at the moorings along 80.5°E shows that the horizontal velocities within the 10–15 day period band are significantly coherent off the equator but not on the equator (Figure 7a). The phase lag between the depth-averaged horizontal velocities at the off equatorial mooring sites is $\pi/2$, with $\overline{v}$ leading $\overline{u}$ in the Northern Hemisphere and $\overline{v}$ lagging $\overline{u}$ in the Southern Hemisphere (Figure 7b). On the equator, the uncertainty of the phase lag is large, consistent with the corresponding insignificant coherence amplitude there. The degree of coherence and respective phase lags between the orthogonal horizontal velocity components reflect the attributes of mixed Rossby-gravity wave. It is clear from Equations 1 and 2 that u is zero on the equator, v leads u by $\pi/2$ in the Northern Hemisphere ($y > 0$), and v lags u by $\pi/2$ in the Southern Hemisphere ($y < 0$).

Using the spectral amplitudes and phases inferred from a rotary spectral analysis of the $\overline{u}\hat{x} + \overline{v}\hat{y}$ time series from the moorings along 80.5°E, we determined the lengths of the semi-minor and major axes of the water particle motions for a set of frequencies resolved by the spectral analysis. The axis ratio between the semi-minor over the semi-major axis at different latitudes along 80.5°E for the nominal biweekly frequency of 1/14-days is shown in Figure 7c. The meridional structure of the ratio for the water particle path of mixed Rossby-gravity wave, following Equations 1 and 2, is given as

$$\frac{u}{v}(y) = \frac{-\omega y}{c}. \tag{3}$$

Applying the least squares technique, we fit the meridional structure of the observed axis ratio (dots in Figure 7c) to Equation 3 with ω set to 1/14-days and find a value of $c \sim 1.4 \pm 0.2$ m s^{-1}. Thus, our c estimates from both Equation 3 and the orthogonal functions of Equations 1 and 2 closely match the theoretical value for a second baroclinic mixed Rossby-gravity wave mode. The trapping distance of a Rossby-gravity wave is controlled by the values of c, with $L = \sqrt{\frac{c}{\beta}}$. By using the c estimates, ranging between 1.4 ± 0.2 m s^{-1} and 1.8 ± 0.4 m s^{-1}, we found that the trapping distance or e-folding scale for biweekly mixed Rossby-gravity wave along 80.5°E varies between 228 and 309 km. The observed biweekly horizontal currents along 80.5°E are thus unlikely to be significantly affected by the Sri Lanka coast, which is about 600 km north of the equator.

4. Phase and Energy Propagation of the Biweekly Waves

Biweekly variability is a prominent mode in v not only at the mooring sites along 80.5°E but also at the 78°E, 83°E, and 90°E equatorial mooring sites (Figures 3a, 3c, and 3d). To probe the role of the biweekly Rossby-gravity wave in accounting for the covariance between v along the equator, we regressed the biweekly v

variability at the equatorial moorings against the principal component of the leading bivariate EOF mode of the velocities from the moorings along 80.5°E. The regressed v, scaled to standard deviation of the principal component, highlights a significant covariance between the biweekly mode along 80.5°E and at other locations along the equator (Figure 8). These results indicate that a northward v at 80.5°E lags that at 90°E by 4.2 ± 0.4 days, on average across the upper 150 m, which implies that the observed Rossby-gravity waves propagate westward along the equator with a zonal phase speed (c_x) of 2.9 ± 0.3 m s^{-1}.

The regressed v on the equator provides insight into the vertical structure of the current velocity associated with the biweekly Rossby-gravity wave. A gradual upward phase shift, with deeper levels leading shallower levels, indicates upward phase propagation with a vertical phase speed (c_z) of about 56 ± 5 m day^{-1} (Figure 8; Table 1), which is inferred from the slope of the linear least squares fit to the regressed v peaks, with the uncertainty denoting a 95% confidence level. The presence of vertical phase propagation indicates that more than one baroclinic mode must be present, since individual vertical mode motions are perfectly in or out of phase as a function of depth (e.g., McCreary, 1984). This result does not invalidate the inference that the second baroclinic mode is dominant based on the results of the previous section. In fact, the observed zero crossing at a depth of around 175–200 m in regressed biweekly v at 0°, 80°E (Figure 8b) occurs at the zero-crossing depth expected for a second baroclinic mode in the Indian Ocean of 175 m based on our normal mode decomposition. We thus conclude that the observed vertical phase propagation reflects the presence of multiple vertical modes, of which the second is dominant.

Observations of horizontal velocities in the upper 220 m at the zonally separated sites allow comparison with the dispersion relation for zonally and vertically propagating equatorial waves. The observed horizontal dispersion relation (ω–k) can be derived via a coherence analysis of $\overline{v}$ from multiple pairs of mooring sites zonally separated by a distance (d) along the equator. The analysis results in a set of coherence amplitude and phase (α) estimates at a discrete set of frequencies (ω). Taking into account only the phase information when the respective coherence amplitude exceeds the 95% significance level, we determined the zonal wavenumber (k) as $k(\omega) = \dfrac{\alpha(\omega)}{d}$ for the biweekly period band.

The observed ω–k scatter generally clusters around the theoretical dispersion curves for the gravest three baroclinic Rossby-gravity waves (Figure 9a), whose dispersion relation in the zonal direction can be represented from theory as

$$k = \frac{\omega}{c} - \frac{\beta}{\omega}. \tag{4}$$

The least squares fit (gray curve in Figure 9a), inferred from fitting Equation 4 to the observed ω–k, falls in between the dispersion curves for the first two baroclinic modes. The c value inferred from the fit is 2.0 ± 0.2 m s^{-1}, similar to that inferred from the meridional structure of the leading bivariate EOF mode of the biweekly variability in $\overline{v}$ and $\overline{u}$ along 80.5°E (Table 1). Compared to the theoretical dispersion relation for equatorial waves, the inferred ω - k estimates in the biweekly period band are distinctively different from those of Kelvin and low frequency Rossby waves.

Based on the least squares fit of the observed dispersion diagram, a Rossby-gravity wave oscillating with ω of 2π/14-days corresponds with a k value of $-1.8 \pm 0.25 \times 10^{-6}$ rad m^{-1}, equivalent to a zonal wavelength (λ_x) of 3,430 ± 550 km (orange square in Figure 9a; Table 1). The average magnitude of the observed k values across the biweekly period band is $-1.6 \pm 0.25 \times 10^{-6}$ rad m^{-1}. Using the k magnitude for ω of 2π/14-days, we find that biweekly mixed Rossby-gravity waves propagate with a zonal phase speed $\left(c_x = \dfrac{\omega}{k}\right)$ of -2.8 ± 0.4 ms^{-1} (Table 1), with the negative sign denoting westward propagation.

As evident from the observed meridional structure of $\overline{v}$ and $\overline{u}$ and ω–k dispersion curve (Figures 5 and 9a), the bulk of the biweekly variability of the observed horizontal currents is attributable to the gravest two or three baroclinic mixed Rossby-gravity wave modes, with the second mode dominating. The presence of multiple baroclinic wave modes leads to vertical propagation of both phase and energy. Following Gill (1982), the dispersion relation for vertically propagating mixed Rossby-gravity waves can be expressed as

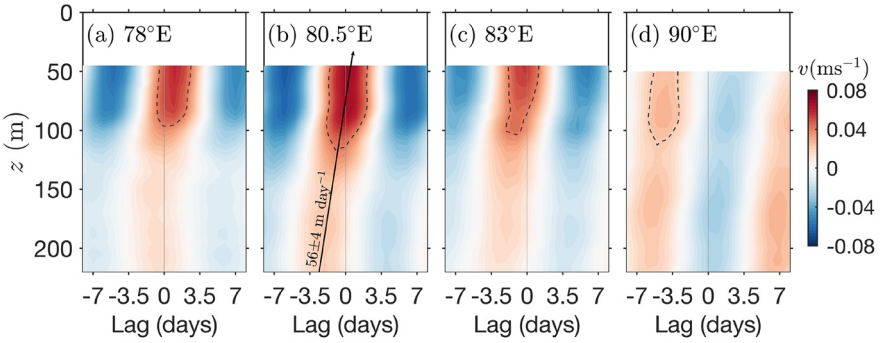

Figure 8. Regressed v at equatorial mooring sites against the principal component of the first bivariate EOF of $\overline{u}$ and $\overline{v}$ along 80.5°E in the 10–15 day period band, scaled to one standard deviation of the principal component. Negative lags indicate that the principal component leads v at 80.5°E, while positive lags denote that the principal component lags v at 80.5°E. Dashed contours mark the $v = 0.04$ m s^{-1} contour in (a–c) and the $v = 0.02$ m s^{-1} contour in (d). Black line with an arrow at its end in (b) is a linear least squares fit to the regressed v peaks, marking the direction of vertical phase propagation, and its slope infers the vertical phase speed estimate. White areas indicate values below 95% significance level.

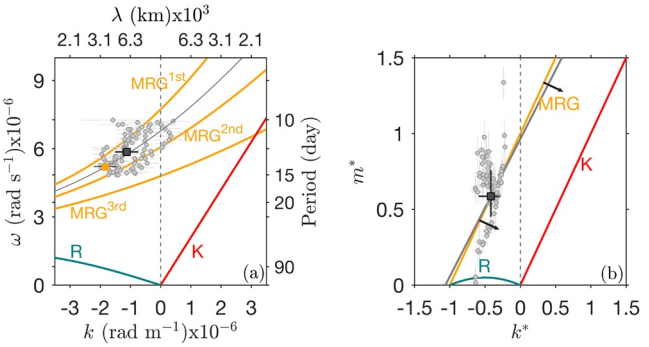

Figure 9. (a) Dispersion diagram (ω–k) for the first three vertical mode mixed Rossby-gravity waves (MRG; orange) based on values for c of 2.6, 1.6, and 1.0 m s^{-1}, respectively, determined from hydrography. Dots represent observed frequency-wavenumber pairs inferred from zonal coherence of $\overline{v}$ at the 78°E, 80.5°E, 83°E, and 90°E equatorial moorings. Gray curve shows the least squares fit of the dispersion relation of mixed Rossby-gravity wave to the dots. The inferred value of c based on this fit is 2.0 ± 0.2 m s^{-1}, which is used to plot the dispersion curves for the Kelvin wave (K, red) and Rossby wave (R, green). (b) Nondimensionalized dispersion curves (m^*–k^*) for vertically propagating equatorially trapped waves with $\omega = 2\pi/14$-days. Dots mark (m^*, k^*) pairs based on observed vertical and zonal structures. Like k, its nondimensional form $\left(k^* = \frac{k\omega}{\beta}\right)$ is determined from zonal coherence of $\overline{v}$ at different equatorial moorings, while its corresponding vertical wave number $\left(m^* = \frac{\omega^2}{\beta N}\right)$ is determined from the vertical coherence of v at 50 and 150 m for each of the moorings. Gray curve shows the linear least squares fit to the dots. Black arrows indicate the propagation direction of the mixed Rossby-gravity wave group velocity. Black squares and horizontal and vertical bars in (a and b), respectively denote the average values and the 95% confidence limits. Orange square marks the ω–k value on the least squares fit for $\omega = 2\pi/14$-days. Positive values of k or k^* and m^* indicate eastward and upward phase propagation, respectively while negative values indicate westward and downward phase propagation.

$$k = \frac{|m|\omega}{N} - \frac{\beta}{\omega} \tag{5}$$

where m is vertical wavenumber. This equation can be nondimensionalized as

$$k^* = m^* - 1 \tag{6}$$

with $k^* = \frac{k\omega}{\beta}$ and $m^* = \frac{m\omega^2}{\beta N}$.

Applying a coherence analysis method similar to that used to estimate k, we determined k and m from coherence phases of v observed at 50 and 150 m from multiple pairs of zonally separated equatorial moorings. The k and m were then nondimensionalized to determine k^* and m^* by setting $N = 0.017$ s^{-1}, an average N value in the upper 150 m in the region 5°N-5°S and 76°E-92°E, and $\omega = 2\pi/14$-days. Like the ω–k dispersion curve, the observed values of m^* and k^* for the biweekly variations (dots in Figure 9b) are scattered around the dispersion curve of mixed Rossby-gravity wave, with m^* positive and k^* negative, indicating westward and upward phase propagation. The observed dispersion diagram differs from the theoretical curves for vertically propagating Kelvin and Rossby waves (Figure 9b). The average m^* value for $\omega = 2\pi/14$-days is 0.59 ± 0.12, which dimensionally implies an average m, vertical wavelength (λ_z), and phase speed c_z of 0.0083 ± 0.001 rad m^{-1}, 760 ± 150 m, 54 ± 6 m day^{-1}, respectively (Table 1). The average c_z estimate is within the error limits of that derived from the vertical structure of the regressed v along the equator shown in Figure 8.

The group velocity (c_g) of the waves is, by definition, directed at the right angles to the m–k dispersion curves of the waves and in the direction of increasing ω (Gill, 1982). Following the definition, c_g for the observed biweekly mixed Rossby-gravity waves is directed downward and eastward

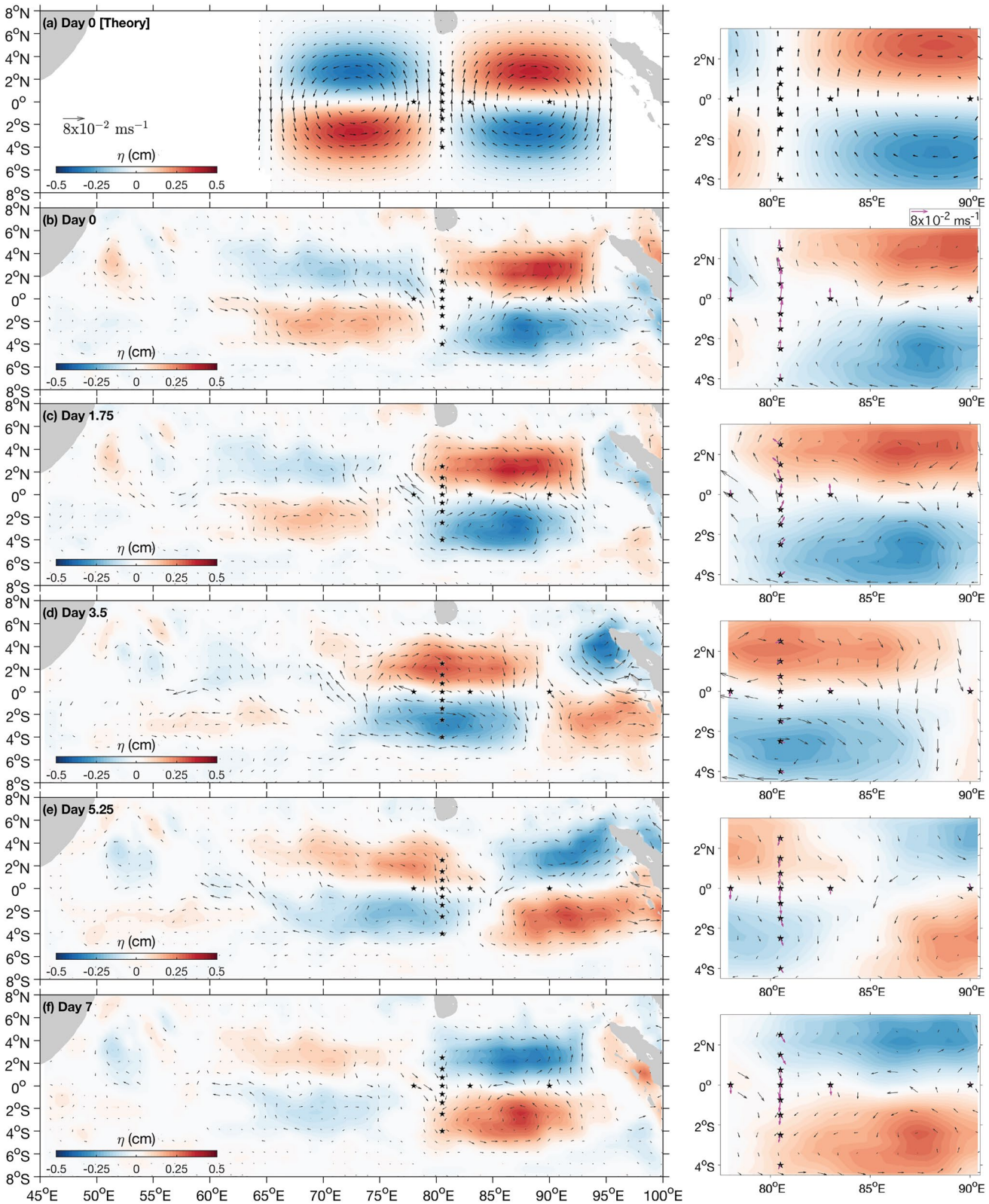
(a) Day 0 [Theory]
(b) Day 0
(c) Day 1.75
(d) Day 3.5
(e) Day 5.25
(f) Day 7
8x10^-2 ms^-1
η (cm)
-0.5 -0.25 0 0.25 0.5
8°N 6°N 4°N 2°N 0° 2°S 4°S 6°S 8°S
45°E 50°E 55°E 60°E 65°E 70°E 75°E 80°E 85°E 90°E 95°E 100°E
2°N 0° 2°S 4°S
80°E 85°E 90°E

as indicated by the arrows in Figure 9b. Its vector is the gradient of ω in wavenumber space, that is a partial derivative of Equation 5 with respect to k and m, given as

$$\overrightarrow{c_g} = \frac{\partial \omega}{\partial k}\hat{x} + \frac{\partial \omega}{\partial m}\hat{z} = \frac{1}{|m|\omega^2 + \beta N}\left(\omega^2 N\hat{x} - \omega^3\hat{z}\right), \tag{7}$$

where $\hat{z}$ is a unit vector in the upward direction. For the observed average value of m and $\omega = 2\pi/14$-days, we determined $\overrightarrow{c_g} = 7.4 \times 10^{-1}$ m s^{-1} $\hat{x}$ -2.3×10^{-4} m s^{-1} $\hat{z}$. The group velocity estimate permits a calculation of the kinetic energy flux per unit horizontal area on the equator (F), that is the product of c_g and energy density. Using a simplified form of the energy flux formula (Eriksen & Richman, 1988; Smyth et al., 2015),

$$F = \rho_o \frac{\sqrt{\pi}}{8} v_o^2 \frac{\omega^3}{\beta N}\mathrm{sgn}(m), \tag{8}$$

we determined that biweekly mixed Rossby-gravity waves over the course of the observation period in the upper 150 m of the equatorial Indian Ocean generate a downward energy flux per unit horizontal area with an average magnitude of 0.08–0.12 mWm^{-2}, where ρ_o or reference density is set 1,024 kg m^{-3}, $v_o = 0.034 \pm 0.003$ m s^{-1}, $\omega = 2\pi/14$-days, and sgn (m) is the sign of m. This magnitude is similar to that reported by Smyth et al. (2015) for a mixed Rossby-gravity wave event with a downward energy flux of 0.16 mWm^{-2} in a layer between 300 and 600 m in the equatorial Indian Ocean. For comparison, the downward energy flux due to near inertial waves in the region is about 1–4 mWm^{-2} (Alford, 2001), over 10 times larger than for mixed Rossby-gravity waves.

5. Basin-Scale Structure of the Biweekly Waves

The observed horizontal moored velocity data provide insights into the three-dimensional structure of biweekly variability in the Indian Ocean and facilitate comparison with the dynamics of the theoretical mixed Rossby-gravity wave. To further illustrate the relationship between the moored velocities and the biweekly Rossby-gravity wave over the broader Indian Ocean, we next regress satellite-derived atmospheric and oceanic parameters onto the principal component of the leading bivariate EOF mode of $\overline{u}$ and $\overline{v}$.

A regression analysis between the principal component of the leading bivariate EOF and both η and GEKCO surface currents reveals a spatial pattern reflective of oceanic mixed Rossby-gravity wave oscillating at a biweekly period in the Indian Ocean (Figures 10b–10f). At day zero, northward symmetric $\overline{v}$ along 80.5°E corresponds to an antisymmetric dipole structure in η about the equator (Figure 10b). Based on the zonal structure of the η pattern, the wave has a zonal wavelength of about 3,850 km, which is within the range of the average zonal wavelength inferred from the observed dispersion diagram (Figure 9a). Moreover, the antisymmetric dipole pattern in η corresponds with clockwise and counterclockwise surface circulations, centered on the equator, to the east and west of the moorings. At day 7 (i.e., after half a wave cycle) when equatorially symmetric $\overline{v}$ is southward along 80.5°E (Figure 10f), the sea level and surface circulation patterns are roughly opposite of what they were at day zero (Figure 10b). The observed patterns generally agree with theory despite showing some noticeable differences such as smaller scale vortical motions embedded in the larger clockwise or anticlockwise circulations (Figures 10a and 10b). Relative to the regressed velocities off equator, the moored and GEKCO velocities on the equator show more noticeable discrepancies, particularly those at 90°E (right panels of Figure 10).

Figure 10. (a) Theoretical structures of η (shading) and surface currents (black arrows) associated with free mixed Rossby-gravity wave when v peaks northward at 80.5°E and day 0, with $c = 2.0$ m s^{-1}, $\lambda_x = 3{,}430$ km, and $\omega = 2\pi/14$-days. Only the structures attributed to one wavelength centered on 80.5°E are shown. (b–f) Evolution of satellite-derived η and GEKCO surface currents (black arrows), regressed against the principal component of the first bivariate EOF of $\overline{u}$ and $\overline{v}$ along 80.5°E at 10–15 day periods and scaled to one standard deviation of the principal component. Right panels show blow-ups of the respective η and surface current plots in the vicinity of the RAMA moorings (stars), with magenta arrows indicating the regressed moored velocities in the biweekly period band averaged over the upper 150 m. Values below the 95% significance level are omitted. The velocity scale on the right panels applies to both the regressed GEKCO and moored velocities. The theoretical wave structure shown in panel (a) was computed in an unbounded basin but the continental boundaries are shown for comparison with the rest of the panels. The black arrows are shown at a 1° × 1° grid for readability.

The time evolution of the η and surface currents exhibits westward phase propagation, as evident in Figures 10c–10f. Applying a linear least squares fit to the time and longitude data from tracking the zonal movement between 80°E and 90°E of a node of the regressed biweekly η averaged between 2°N and 3°N and 2°S and 3°S yields a mean westward phase speed about 3.1 ± 0.3 m s^{-1}. Tracking the node movement from farther east of 90°E results in a lower westward phase speed estimate for reasons that remain unclear. The average westward c_x estimate from the regressed satellite-derived biweekly η is in agreement with that from the regressed vertical structure and zonal dispersion relation of the moored biweekly v along the equator, within the overlapping error bounds of each. Arzeno et al. (2020) reported westward propagating biweekly mixed Rossby-gravity waves in satellite altimetry with a mean phase speed of 3.4 m s^{-1}, which is close to our c_x estimates considering the uncertainties.

The wind stress τ and wind stress curl, regressed against first bivariate EOF of $\overline{u}$ and $\overline{v}$ along 80.5°E, exhibits a strong relationship with surface currents on biweekly timescales (Figure 11). When $\overline{v}$ is northward at day 0 along 80.5°E, local meridional winds are also northward and flanked by two oppositely rotating vortices to the east and west (Figures 11a). The correspondence in direction of local meridional wind stress and currents suggests that the meridional winds are energizing the oceanic mixed Rossby-gravity wave through wind work at the surface, consistent with the numerical experiment results of Sengupta et al. (2004) and Miyama et al. (2006). The regressed τ also demonstrates a wind field with a vortex structure reminiscent of the QBM vortex centered near the equator, albeit with a smaller zonal wavelength of about 4,400 km, as reported in previous studies (e.g., Chatterjee & Goswami, 2004; Chen & Chen, 1993). The wind stress vortex shifts westward consistent with the westward phase propagation of meridional wind stress (Figure 3e) and the southerly wind stress turns to northerly after about a half cycle of the biweekly wave (Figures 11b–11e).

The basin-scale structure and time evolution of the regressed τ partially explain those of the regressed η and surface currents. It appears for example that the η pattern is a response to the negative $\nabla \times \tau$ field-forced Ekman convergence or divergence. A negative wind stress curl field would respectively cause Ekman convergence that elevates sea level in the Northern Hemisphere and Ekman divergence that suppresses sea level in the Southern Hemisphere, while the opposite sign of the curl would excite the opposite η response. Ogata et al. (2008) suggested that Ekman convergence-driven downwelling to the north of the equator and divergence-driven upwelling to the south would result in surface northward cross-equatorial flow.

6. Summary and Discussion

We have used the most comprehensive data set of the moored horizontal velocities in the upper Indian Ocean during September 2008–June 2013, together with satellite and reanalysis products, to provide a detailed assessment of the properties of biweekly variability (at periods ranging between 10 and 15 days) near the equator. By comparing the properties and structure of the observed biweekly flow field from the in situ and satellite measurements, we concluded that wind-forced Rossby-gravity waves are the dominant source of biweekly horizontal current variations in the equatorial Indian Ocean. From mooring data along the equator and along 80.5°E, we find that variance in $\overline{v}$ is maximum on the equator and decays at higher latitudes, while the variance in $\overline{u}$ has a node on the equator and is comparable to or more energetic than that of $\overline{v}$ at the northern and southernmost moorings. A phase shift of $\pi/2$ between $\overline{u}$ and $\overline{v}$ is observed in the off equatorial moorings, with $\overline{v}$ leading $\overline{u}$ in the Northern Hemisphere and $\overline{v}$ lagging $\overline{u}$ in the south. The biweekly flow field is thus rectilinear on the equator and elliptical at higher latitudes.

The leading bivariate EOF mode of the biweekly $\overline{u}$ and $\overline{v}$ along 80.5°E, accounting for 40% of the biweekly variance, best approximates the meridional structures of horizontal currents associated with the mixed Rossby-gravity wave. The Kelvin wave phase speed (or separation constant c) estimated from the least squares fit to the meridional modes are 1.6 ± 0.4 and 1.8 ± 0.4, m s^{-1}, respectively. Likewise, the meridional structure of the semi-minor to semi-major axis ratio of the observed biweekly flow is consistent with that for the Rossby-gravity wave water particle paths, with an inferred c of 1.4 ± 0.2 m s^{-1}. Compared to the representative c values for the gravest four baroclinic modes derived from a normal mode decomposition of a mean stratification frequency profile observed in the tropical Indian Ocean, the c estimates from the moored biweekly flow field are closest to the phase speed for the second baroclinic wave mode.

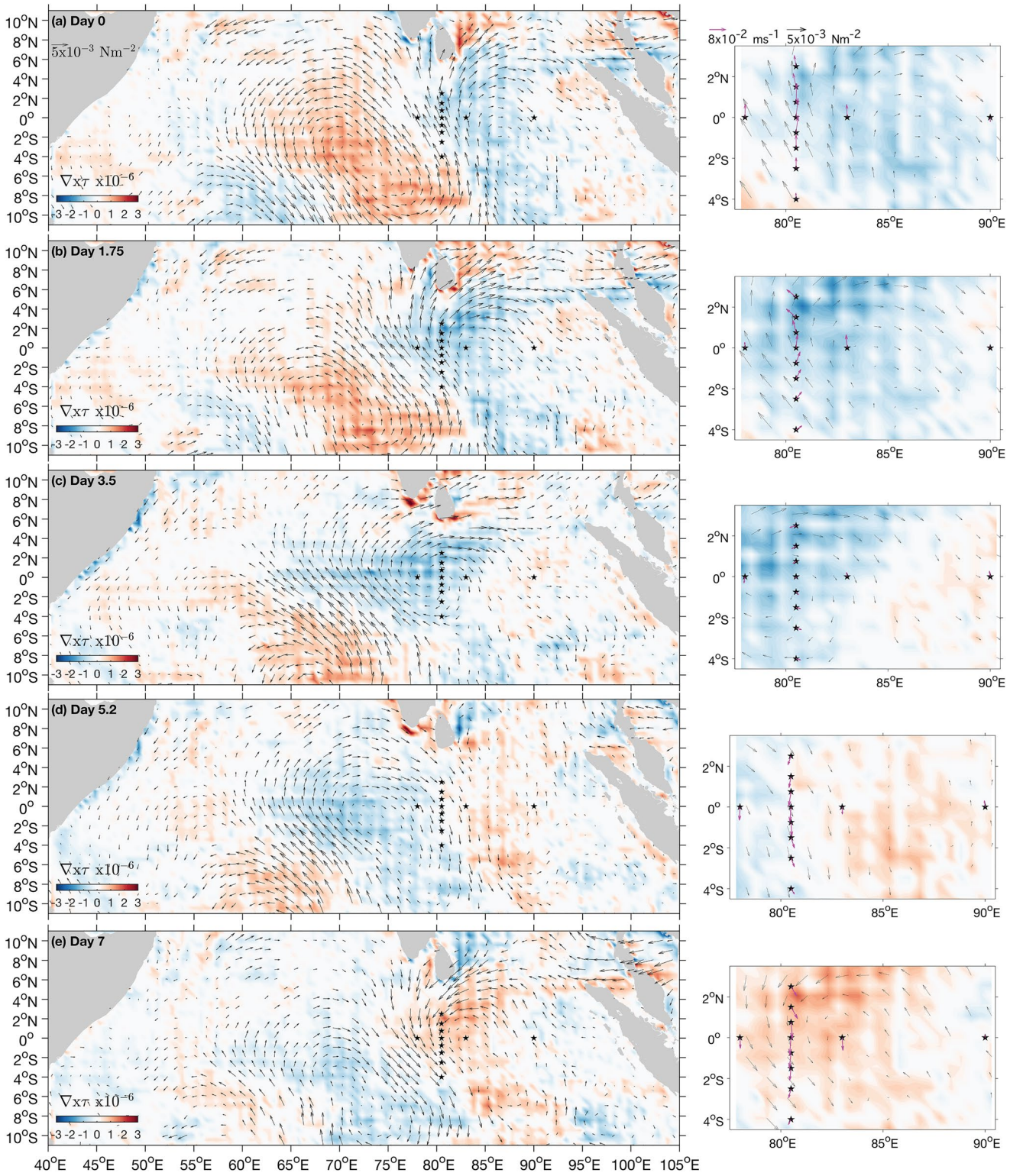

Figure 11. Evolution of $\nabla \times \tau$ (shading) and τ (black arrows), regressed against the principal component of the first bivariate EOF of $\overline{u}$ and $\overline{v}$ along 80.5°E at 10–15 day periods and scaled to one standard deviation of the principal component. Right panels show blow-ups of the respective $\nabla \times \tau$ and τ plots in the vicinity of the moorings (stars), with magenta arrows indicating the regressed moored velocities at the biweekly period band averaged in the upper 150 m. Values below the 95% significance level are omitted. The black arrows are shown at a 1° × 1° grid for readability.

The regressed biweekly v in the upper 220 m on the equatorial moorings at 78°E, 80.5°E, 83°E, and 90°E, against the principal component of the leading bivariate EOF mode of the biweekly $\overline{u}$ and $\overline{v}$ along 80.5°E, exhibits a vertical structure with a zero-crossing depth at about 175–200 m. The vertical structure shows phase propagation from deeper to shallower levels with an average vertical phase speed (c_z) of 56 ± 5 m day^{-1}; variations also exhibit westward zonal phase propagation from the easternmost mooring with an average westward zonal phase speed (c_x) of 2.9 ± 0.3 m s^{-1}.

Based on zonal and vertical coherences of the biweekly $\overline{v}$ at the equatorial moorings, the observed zonal wavenumber-frequency (ω - k) and zonal-vertical wavenumber (m–k) dispersion diagrams compare well with the theoretical dispersion curves for mixed Rossby-gravity wave. The dispersion curve of Rossby-gravity wave with $c = 2.0 \pm 0.2$ m s^{-1} best approximates the observed dispersion zonal diagram. The average λ_x and λ_z values of the observed biweekly Rossby-gravity wave from the dispersion diagrams are respectively 3,430 ± 550 km and 760 ± 150 m. For the average wavelengths and a frequency of 2π/14-days, the wave phase propagates westward and upward with c_x and c_z of 2.8 ± 0.4 m s^{-1} and 54 ± 6 m day^{-1}, respectively. Taking into account the uncertainties, the c_x and c_z estimates are comparable with those obtained from the regressed biweekly v at the equatorial moorings noted above. The wave energy propagates eastward and downward, with the average amount of kinetic energy flux carried downward varying between 0.08 and 0.12 mW m^{-2}, about an order of magnitude smaller than that due to near-inertial waves in the region.

The basin scale temporal evolution of the biweekly mode and its relation to wind stress forcing are well captured by the pattern of satellite-retrieved surface currents, sea level anomaly, and wind stress in the Indian Ocean, regressed against the leading bivariate principal component. The regressed sea level and surface currents illustrate that the biweekly Rossby-gravity waves observed in the Indian Ocean are marked by a mean zonal wavelength and westward phase speed of 3,850 km and 3.1 ± 0.3 m s^{-1}, respectively. Moreover, the regressed wind stress clearly depicts the biweekly vortex centered near the equator and its westward propagation, presumably the primary forcing for the observed biweekly oceanic Rossby-gravity waves.

The meridional structure of mixed Rossby-gravity waves in the Indian Ocean has never been clearly discerned from in situ measurements in past studies. Using observations from an array of moorings along 80.5°E between 1°S and the southern coast of Sri Lanka during July 1993–September 1994, Reppin et al. (1999) reported a notable spectral peak of biweekly variability in the observed horizontal currents but did not describe the cause of the peak. Their study focused more on the variability of the horizontal currents on seasonal and longer time scales. Employing shipboard ADCP data at 80.5°E and the equator and along a couple of transects between 2°N and 2°S observed over the course of October–November 2011, Smyth et al. (2015) described a wavelike feature observed clearest in v on the equator within a layer between 300 and 600 m. Based on the inferred wave properties from the shipboard measurements, they argued that a mixed Rossby-gravity wave pulse with a timescale of about 3 weeks caused the pronounced feature in the deep layer, with estimated horizontal and vertical wavelengths and meridional trapping scale about a fourth to a half of those our observations demonstrate in the upper layer.

There are some other notable discrepancies between our results and past studies, particularly those of numerical-based results. Using model horizontal currents, Sengupta et al. (2004) and Miyama et al. (2006) reported pronounced biweekly mode in near-surface v along the equator, with a gradual increase of biweekly variance from the western Indian Ocean to the eastern basin. They argued that eastward energy propagation attributed to biweekly mixed Rossby-gravity wave explained the largest biweekly variability in the eastern Indian Ocean. In contrast to their model results, our observations show decreasing biweekly variance toward the eastern basin, consistent with the observed zonal variation of the biweekly equatorial meridional wind stress. Earlier observations of v at 80.5°E and 90°E on the equator during October 2004–October 2008 showed a similar decreasing trend of biweekly variance toward the eastern equatorial Indian Ocean (Nagura et al., 2014). A possible source of discrepancy between the observed and model results likely relates to the wind input used in the model. The amplitude of the observed biweekly meridional wind stress decreases toward the east, whereas the wind stress used in Miyama et al. (2006) increases toward the east. Moreover, the wave energy travels eastward and downward along a raypath at group velocity speeds. Thus, biweekly mixed Rossby-gravity waves excited by meridional wind stress variations in the central equatorial Indian

Ocean should cause maximum biweekly variations at depth in the eastern basin rather in the near-surface layer. Using a theoretical raypath of the energy propagation, Ogata et al. (2008) demonstrated that a wind-forced biweekly Rossby-gravity wave emanating from around 83°E would exert energetic biweekly variability at 2,000 m at 90°E.

Our observations agree with the model results that the biweekly variability in the equatorial Indian Ocean is mainly composed of mixed Rossby-gravity waves of the gravest few baroclinic modes. Least squares fits to the observed meridional structures and dispersion curves of the biweekly current velocities imply the separation constant values of 1.4–2.0 m s^{-1}. This range of separation constants closely matches that expected for a second baroclinic mixed Rossby-gravity wave mode, implying the second mode is dominant compared to other low baroclinic modes in accounting for the observed biweekly variability in the equatorial Indian Ocean.

From the moored velocity measurements, we derived zonal phase speeds for the mixed Rossby-gravity wave of 2.9 ± 0.3 m s^{-1} and 2.8 ± 0.4 m s^{-1}, depending on the method. We also found from regressed satellite-derived sea level variations a similar zonal phase speed of 3.1 ± 0.3 m s^{-1} for the biweekly mode. Employing multiyear satellite-retrieved sea level data in the Indian Ocean, Arzeno et al. (2020) suggested a slightly higher estimate of westward phase speed of 3.4 m s^{-1} for mixed Rossby-gravity waves. All these estimates are with a few tenths of a meter per second, providing confidence in the order of magnitude of the phase speed.

Previous studies of biweekly waves in the Indian Ocean have focused in the period band 10–20 days (e.g., Arzeno et al., 2020; Sengupta et al., 2004). We found though that v variance between 1°N and 1°S exhibits a period shift with depth, with the largest variance at periods between 10 and 15 days in the upper 100 m, while it is centered about 20 days at depths between 100 and 150 m. The variance near 20 days may not be directly related to wind forcing, so we restricted our analysis to the 10–15 day period band on the assumption that variance at these periods would be most representative of wind-forced mixed Rossby-gravity waves. However, we repeated all the calculations for the broader 10–20 day period band (Table 1) and found none of the derived wave parameters is statistically different from those we estimated for 10–15 day periods. Thus, our conclusions are not sensitive to the exact definition of what we mean by "biweekly" as long as it contains the variance at 10–15 day periods.

The genesis of the pronounced 20-day variability and why it is confined near the equator below 100 m remains an open question. From numerical experiments, Sengupta et al. (2001), showed that a significant fraction of intraseasonal meridional velocity variance in the upper 300 m of the tropical Indian Ocean is linked to dynamic instability, so this 20-day variability could be related to an instability of the large-scale circulation. Further analysis is needed to define the characteristics of this variability and identify its dynamical origins.

Data Availability Statement

RAMA data can be downloaded via https://www.pmel.noaa.gov/tao/drupal/disdel/, and the satellite-derived and GEKCO current data are available in http://marine.copernicus.eu/services-portfolio/access-to-products/ and http://ctoh.legos.obs-mip.fr/data/global-surface-currents/global-surface-current-data-product. Argo profiler data can be obtained from http://www.argodatamgt.org/Access-to-data/Argo-data-selection.

This research was performed while the first author held a National Research Council Research Associateship Award at NOAA/PMEL. MJM is supported by NOAA. This is PMEL contribution 5118.

Acknowledgments
The authors thank three anonymous reviewers for the constructive comments on earlier versions of the manuscript. The authors acknowledge NOAA and its partners for maintaining the RAMA moored buoy array.

References

Alford, M. H. (2001). Internal swell generation: The spatial distribution of energy flux from the wind to mixed layer near-inertial motions. *Journal of Physical Oceanography*, *31*(8), 2359–2368. https://doi.org/10.1175/1520-0485(2001)031<2359:isgtsd>2.0.co;2

Arzeno, I. B., Giddings, S. N., Pawlak, G., & Pinkel, R. (2020). Generation of Quasi-Biweekly Yanai Waves in the Equatorial Indian Ocean. *Geophysical Research Letters*, *47*(16), e2020GL088915. https://doi.org/10.1029/2020GL088915

Bentamy, A., Katsaros, K., Drennan, W., & Forde, E. (2002). Daily surface wind fields produced by merged satellite data. *Gas Transfer at Water Surfaces*, *127*, 343–349. https://doi.org/10.1029/GM127p0343

Chatterjee, P., & Goswami, B. N. (2004). Structure, genesis and scale selection of the tropical quasi-biweekly mode. *Quarterly Journal of the Royal Meteorological Society*, *130*(599), 1171–1194. https://doi.org/10.1256/qj.03.133

Chen, T.-C., & Chen, J.-M. (1993). The 10–20-day mode of the 1979 Indian monsoon: Its relation with the time variation of monsoon rainfall. *Monthly Weather Review*, *121*(9), 2465–2482. https://doi.org/10.1175/1520-0493(1993)121<2465:tdmoti>2.0.co;2

Eriksen, C. C., & Richman, J. G. (1988). An estimate of equatorial wave energy flux at 9- to 90-day periods in the central Pacific. *Journal of Geophysical Research*, *93*(C12), 15455–15466. https://doi.org/10.1029/jc093ic12p15455

Farrar, J. T., & Durland, T. S. (2012). Wavenumber-frequency spectra of inertia-gravity and mixed Rossby-gravity waves in the equatorial Pacific Ocean. *Journal of Physical Oceanography*, *42*(11), 1859–1881. https://doi.org/10.1175/jpo-d-11-0235.1

Gill, A. E. (1982). *Atmosphere-ocean dynamics* (p. 662). Academic Press.

Johnson, E. S., & Mc Phaden, M. J. (1993). Structure of intraseasonal Kelvin waves in the equatorial Pacific Ocean. *Journal of Physical Oceanography*, *23*(4), 608–625. https://doi.org/10.1175/1520-0485(1993)023<0608:soikwi>2.0.co;2

Kikuchi, K., & Wang, B. (2009). Global perspective of the quasi-biweekly oscillation. *Journal of Climate*, *22*(6), 1340–1359. https://doi.org/10.1175/2008jcli2368.1

Krishnamurti, T. N., & Ardanuy, P. (1980). The 10 to 20-day westward propagating mode and "Breaks in the Monsoons". *Tellus*, *32*(1), 15–26. https://doi.org/10.3402/tellusa.v32i1.10476

Masumoto, Y., Hase, H., Kuroda, Y., Matsuura, H., & Takeuchi, K. (2005). Intraseasonal variability in the upper layer currents observed in the eastern equatorial Indian Ocean. *Geophysical Research Letters*, *32*(2). https://doi.org/10.1029/2004gl021896

McCreary, J. P. (1984). Equatorial beams. *Journal of Marine Research*, *42*(2), 395–430.

McPhaden, M. J. (1982). Variability in the central equatorial Indian Ocean. I: Ocean dynamics. *Journal of Marine Research*, *40*, 157–176.

McPhaden, M. J., Meyers, G., Ando, K., Masumoto, Y., Murty, V. S. N., Ravichandran, M., et al. (2009). RAMA: The research moored array for African–Asian–Australian monsoon analysis and prediction. *Bulletin of the American Meteorological Society*, *90*(4), 459–480. https://doi.org/10.1175/2008bams2608.1

McPhaden, M. J., Wang, Y., & Ravichandran, M. (2015). Volume transports of the Wyrtki jets and their relationship to the Indian Ocean Dipole. *Journal of Geophysical Research: Oceans*, *120*(8), 5302–5317. https://doi.org/10.1002/2015jc010901

Miyama, T., McCreary, J. P., Jr., Jensen, T. G., Loschnigg, J., Godfrey, S., & Ishida, A. (2003). Structure and dynamics of the Indian-Ocean cross-equatorial cell. *Deep Sea Research Part II: Topical Studies in Oceanography*, *50*(12–13), 2023–2047. https://doi.org/10.1016/s0967-0645(03)00044-4

Miyama, T., McCreary, J. P., Sengupta, D., & Senan, R. (2006). Dynamics of biweekly oscillations in the equatorial Indian Ocean. *Journal of Physical Oceanography*, *36*(5), 827–846. https://doi.org/10.1175/jpo2897.1

Nagura, M., Masumoto, Y., & Horii, T. (2014). Meridional heat advection due to mixed Rossby gravity waves in the equatorial Indian Ocean. *Journal of Physical Oceanography*, *44*(1), 343–358. https://doi.org/10.1175/jpo-d-13-0141.1

Nagura, M., & McPhaden, M. J. (2008). The dynamics of zonal current variations in the central equatorial Indian Ocean. *Geophysical Research Letters*, *35*(23). https://doi.org/10.1029/2008gl035961

Nagura, M., & McPhaden, M. J. (2010). Dynamics of zonal current variations associated with the Indian Ocean dipole. *Journal of Geophysical Research: Oceans*, *115*(C11). https://doi.org/10.1029/2010jc006423

Ogata, T., Sasaki, H., Murty, V. S. N., Sarma, M. S. S., & Masumoto, Y. (2008). Intraseasonal meridional current variability in the eastern equatorial Indian Ocean. *Journal of Geophysical Research: Oceans*, *113*(C7). https://doi.org/10.1029/2007jc004331

Percival, D. B., & Walden, A. T. (1993). *Spectral analysis for physical applications*. Cambridge University Press.

Pujiana, K., & McPhaden, M. J. (2020). Intraseasonal Kelvin waves in the equatorial Indian Ocean and their propagation into the Indonesian seas. *Journal of Geophysical Research: Oceans*, *125*(5), e2019JC015839. https://doi.org/10.1029/2019jc015839

Pujiana, K., Moum, J. N., & Smyth, W. D. (2018). The role of turbulence in redistributing upper-ocean heat, freshwater, and momentum in response to the MJO in the equatorial Indian Ocean. *Journal of Physical Oceanography*, *48*(1), 197–220. https://doi.org/10.1175/jpo-d-17-0146.1

Reppin, J., Schott, F. A., Fischer, J., & Quadfasel, D. (1999). Equatorial currents and transports in the upper central Indian Ocean: Annual cycle and interannual variability. *Journal of Geophysical Research*, *104*(C7), 15495–15514. https://doi.org/10.1029/1999jc900093

Roman-Stork, H. L., Subrahmanyam, B., & Trott, C. B. (2020). Monitoring intraseasonal oscillations in the Indian Ocean using satellite observations. *Journal of Geophysical Research: Oceans*, *125*(2), e2019JC015891. https://doi.org/10.1029/2019JC015891

Schott, F. A., Xie, S.-P., & McCreary, J. P., Jr. (2009). Indian Ocean circulation and climate variability. *Reviews of Geophysics*, *47*(1). https://doi.org/10.1029/2007RG000245

Sengupta, D., Senan, R., & Goswami, B. N. (2001). Origin of intraseasonal variability of circulation in the tropical central Indian Ocean. *Geophysical Research Letters*, *28*(7), 1267–1270. https://doi.org/10.1029/2000gl012251

Sengupta, D., Senan, R., Murty, V. S. N., & Fernando, V. (2004). A biweekly mode in the equatorial Indian Ocean. *Journal of Geophysical Research: Oceans*, *109*(C10). https://doi.org/10.1029/2004jc002329

Shinoda, T. (2010). Observed dispersion relation of Yanai waves and 17-day tropical instability waves in the Pacific Ocean. *Sola*, *6*, 17–20. https://doi.org/10.2151/sola.2010-005

Smyth, W. D., Durland, T. S., & Moum, J. N. (2015). Energy and heat fluxes due to vertically propagating Yanai waves observed in the equatorial Indian Ocean. *Journal of Geophysical Research: Oceans*, *120*(1), 1–15. https://doi.org/10.1002/2014jc010152

Subrahmanyam, B., Trott, C. B., & Murty, V. S. N. (2018). Detection of intraseasonal oscillations in SMAP salinity in the Bay of Bengal. *Geophysical Research Letters*, *45*(14), 7057–7065. https://doi.org/10.1029/2018gl078662

Sudre, J., Maes, C., & Garçon, V. (2013). On the global estimates of geostrophic and Ekman surface currents. *Limnology & Oceanography*, *3*(1), 1–20. https://doi.org/10.1215/21573689-2071927

Sudre, J., & Morrow, R. A. (2008). Global surface currents: A high-resolution product for investigating ocean dynamics. *Ocean Dynamics*, *58*(2), 101. https://doi.org/10.1007/s10236-008-0134-9

Thomson, R. E., & Emery, W. J. (2014). Chapter 5 – Time series analysis methods. In R. E. Thomson, & W. J. Emery (Eds.), *Data analysis methods in physical oceanography* (3rd ed., pp. 425–591). Elsevier.

Wang, Y., & McPhaden, M. J. (2017). Seasonal cycle of cross-equatorial flow in the central Indian Ocean. *Journal of Geophysical Research: Oceans*, *122*(5), 3817–3827. https://doi.org/10.1002/2016jc012537

Weisberg, R. H., Horigan, A., & Colin, C. (1979). Equatorially trapped Rossby-gravity wave-propagation in the Gulf of Guinea. *Journal of Marine Research*, *37*(1), 67–86.

Wheeler, M. C., & McBride, J. L. (2005). Australian-Indonesian monsoon. In W. K. M. Lau, & D. E. Waliser (Eds.), *Intraseasonal Variability in the Atmosphere-Ocean Climate System* (pp. 125–173). Berlin: Springer.

Wyrtki, K. (1973). An equatorial jet in the Indian Ocean. *Science*, *181*(4096), 262–264. https://doi.org/10.1126/science.181.4096.262

Zhang, C. (2013). Madden-Julian oscillation: Bridging weather and climate. *Bulletin of the American Meteorological Society*, *94*(12), 1849–1870. https://doi.org/10.1175/bams-d-12-00026.1

Zhu, X.-H., Kaneko, A., Gohda, N., Inaba, H., Kutsuwada, K., & Radenac, M.-H. (1998). Observation of mixed Rossby-gravity waves in the western equatorial Pacific. *Journal of Oceanography*, *54*(2), 133–141. https://doi.org/10.1007/bf02751689